HHS Public Access

Author manuscript

Drug Alcohol Depend. Author manuscript; available in PMC 2021 November 01.

Published in final edited form as:

Drug Alcohol Depend. 2020 November 01; 216: 108309. doi:10.1016/j.drugalcdep.2020.108309.

Contrasting Effects of Adolescent and Early-Adult Ethanol Exposure on Prelimbic Cortical Pyramidal Neurons

Ewa Galaj[a], **Changyong Guo**[b], **Donald Huang**[b,c], **Robert Ranaldi**[d], **Yao-Ying Ma**[a,b,c]

[a]Department of Psychology, Behavioral Neuroscience Program, State University of New York, Binghamton, New York 13902, USA

[b]Department of Pharmacology and Toxicology, Indiana University School of Medicine, Indianapolis, IN 46202, USA.

[c]Stark Neurosciences Research Institute, Indiana University School of Medicine, Indianapolis, IN 46202, USA.

[d]Department of Psychology, Queens College, City University of New York, Flushing, New York 11367, USA

Abstract

Background: Adolescence and early-adulthood are vulnerable developmental periods during which binge drinking can have long-lasting effects on brain function. However, little is known about the effects of binge drinking on the pyramidal cells of the prelimbic cortex (PrL) during early and protracted withdrawal periods.

Methods: In the present study, we performed whole-cell patch clamp recordings and dendritic spine staining to examine the intrinsic excitability, spontaneous excitatory post-synaptic currents (sEPSCs), and spine morphology of pyramidal cells in the PrL from rats exposed to chronic intermittent ethanol (CIE) during adolescence or early-adulthood.

Results: Compared to chronic intermittent water (CIW)-treated controls, the excitability of PrL-L5 pyramidal neurons was significantly increased 21 days after adolescent CIE but decreased 21 days after early-adult CIE. No changes of excitability in PrL Layer (L) 5 were detected 2 days after either adolescent or early-adulthood CIE. Interestingly, decreases in sEPSC amplitude and increases in thin spines ratio were detected 2 days after adolescent CIE. Furthermore, decreased frequency and amplitude of sEPSCs, accompanied by a decrease in the density of total spines and non-thin spines were observed 21 days after adolescent CIE. In contrast, increased frequency and amplitude of sEPSCs, accompanied by increased densities of total spines and non-thin spines were found 21 days after early adult CIE.

Corresponding author: Dr. Yao-Ying Ma, Department of Pharmacology and Toxicology, Indiana University School of Medicine 635 Barnhill Drive, Indianapolis, IN 46202, Tel: 317-274-1536, Fax: 317-274-7714, ym9@iu.edu.

Author contributions EG, CG, RR and YM were responsible for experimental design. EG, CG and DH were responsible for data collection. EG, CG, RR and YYM were responsible for data analysis and paper drafting.

Conflict of interest The authors report no conflicts of interest.

Conclusion: CIE produced prolonged neuronal and synaptic alterations in PrL-L5, and the developmental stage, i.e., adolescence vs. early-adulthood when subjects receive CIE, is a key factor in determining the direction of these changes.

Keywords

adolescence; early-adulthood; chronic intermittent ethanol; dendritic spine; intrinsic excitability; excitatory post-synaptic current; prelimbic cortex

1. Introduction

Alcohol is the most widely abused substance in the world. In fact, alcohol abuse is more widespread than all other drugs combined (Witt, 2010). Most people in the United States begin to use alcohol during adolescence or early-adulthood (National Institute on Alcohol Abuse and Alcoholism, 2017; Sloan et al., 2011; Spear and Swartzwelder, 2014). Young-age alcohol-drinking is a serious public health concern, with 7.7 million individuals between the ages of 12–20 years reporting drinking alcohol within the past month (Substance Abuse and Mental Health Services Administration, 2015). In particular, binge-drinking episodes were reported at least once in the previous month by 5.1 million underage drinkers and over 90% of alcohol consumed by underage drinkers was in the form of binge-drinking episodes (National Institute on Alcohol Abuse and Alcoholism, 2017). This high prevalence of binge alcohol drinking occurs at a critical period during development when the central nervous system is undergoing rapid adaptations in structure and function that may lead to subsequent susceptibility to neuropsychiatric disorders. The behavioral consequences, especially the prolonged effects of adolescent/young adult alcohol exposure in the clinic cause substantial morbidity, but available treatments are limited (Kyzar et al., 2019; Sakharkar et al., 2019; Viner and Taylor, 2007). One reason is the lack of sufficient understanding about the neuronal alterations induced by adolescent/young adult binge alcohol exposure, and how these changes contribute to the increased risk of alcohol abuse-related neuropsychiatric disorders, even after a prolonged withdrawal period.

The prelimbic cortex (PrL), as part of the medial prefrontal cortex, is particularly vulnerable to alcohol exposure during adolescence as it shows a much slower rate of maturation compared with other brain regions. The stabilization and final maturation of the PrL is assumed to be achieved until the third decade of human life (Petanjek et al., 2011). Thus, neuronal alterations and synaptic pruning are still ongoing not only during adolescence but also during early adulthood. In addition, lamination is the key architectural feature of the cerebral neocortex. As cortical maturation occurs in an inside-out fashion, layer-specific alterations (Cooper, 2008) can be expected when immature brains are exposed to alcohol. The difference between superficial layers (primarily layer 2/3, denoted as L2) and the deeper layers (layer 5, L5, in particular) has been extensively explored in alcohol/ethanol-free subjects (Harris and Shepherd, 2015; Lefort et al., 2009; Rolls, 2016). Besides extrinsic inputs, L2 receives cortical inputs from other layers except L5 and projects to L5 as well as other layers. In contrast, L5, as the dominant output to subcortical and other cortical regions, broadly integrates the inputs from all the other layers including L2 (D'Souza and Burkhalter, 2017). Thus, besides the significant overlap in their anatomical networks and biological

functions, L2 and L5 may play differential roles by gathering information and generating outputs, respectively.

Binge-like ethanol exposure in laboratory animals has been modeled by chronic intermittent ethanol (CIE) administration, which could help in our understanding of potential mechanisms. The developmental stage-dependent and layer-specific effects of CIE are explored in the current studies. Specifically, the effects of CIE on neuronal excitability, spontaneous excitatory postsynaptic currents (sEPSCs), and spine morphology of PrL-L2 *vs.* PrL-L5 during both adolescence (P28–45, denoted "Ado") and early-adulthood (P70–88, denoted "Adu") are explored at 2 days and 21 days after the last alcohol exposure. Our results reveal important differences in neuronal excitability, synaptic transmission, and spine morphology that are developmental stage- and layer-specific.

2. Materials and methods

2.1. Animals

All procedures were performed in accordance with the United States Public Health Service Guide for Care and Use of Laboratory Animals and were approved by the Institutional Animal Care and Use committees at the State University of New York, Binghamton and Indiana University School of Medicine. Experiments were conducted on male Sprague-Dawley rats, bred in-house using breeders originally derived from Envigo, USA. With the day of birth being deemed as P0, rats were weaned at P21–23 and pair-housed in standard Plexiglas cages. Rats were maintained on a 7 AM / 7 PM light / dark schedule with *ad libitum* access to food and water. Rats were handled to habituate them to human contact prior to experimentation. In total 124 male rats, randomly picked up from ~60 litters, were used in this study.

2.2. Chronic intermittent ethanol exposure

Our CIE procedure was described in our recent publication (Shan et al., 2019). Briefly, adolescent (Ado, P28-P45) or early adult (Adu, P70-P88) rats received 4.0 g/kg intragastric (IG) administration of 25% (v/v) ethanol (CIE) or equivalent volume of water (CIW) once per day at approximately 9:00 AM in a 3-day on and 2-day off pattern as one cycle, repeated 4 times in total as illustrated by Fig. 1A. This CIE was verified as an effective procedure of alcohol binge exposure (defined as >80 mg/dL by NIAAA) in our previous publication (Shan et al., 2019). In order to avoid the potential stress induced by tail blood withdrawal, ethanol concentration measurement was not performed in the animals used in the current studies.

2.3. Brain slice whole-cell patch clamp recordings

Standard procedures were used for preparing slices and whole-cell patch clamp recordings as detailed in our previous publications (Ma et al., 2012; Ma et al., 2014). Before sacrifice, the rats were anesthetized with isoflurane and subsequently transcardially perfused with 4°C cutting solution (in mM: 135 *N*-methyl-D-glucamine, 1 KCl, 1.2 KH_2PO_4, 0.5 $CaCl_2$, 1.5 $MgCl_2$, 20 choline-HCO_3, 11 glucose, pH adjusted to 7.4 with HCl, and saturated with 95% O_2 /5% CO_2). The rat was decapitated, and then the brain was removed and glued to a block

before slicing using a Leica VT1200s vibratome in 4°C cutting solution. Coronal slices of 250-μm thickness were cut such that the preparation contained the signature anatomical landmarks (e.g., the rhinal fissure, the anterior commissure and the corpus callosum as shown in Fig. 1B) that clearly delineate the PrL area (between +3.5 to +2.5 mm from bregma; 0.25–0.35 mm from the pial surface for L2 and 0.80–1.00 mm from the pial surface for L5) (Paxinos and Watson, 2007). After allowing at least 1 hr for recovery, slices were transferred from a holding chamber to a submerged recording chamber where it was continuously perfused with oxygenated ACSF maintained at 30 ± 1°C.

Standard whole-cell current- or voltage-clamp recordings were obtained with a MultiClamp 700B amplifier (Molecular Devices), filtered at 3 kHz, amplified 5 times, and then digitized at 20 kHz with a Digidata 1550B analog-to-digital converter (Molecular Devices). The recording electrodes (3–5 MΩ) were filled with (in mM): 108 $KMeSO_3$, 20 KCl, 0.4 K-EGTA, 10 Hepes, 2.5 Mg-ATP, 0.25 Na-GTP, 7.5 phosphocreatine (2Na), 1 L-glutathione, 2 $MgCl_2$, pH 7.3. The recording bath solution contained (in mM): 119 NaCl, 2.5 KCl, 2.5 $CaCl_2$, 1.3 $MgCl_2$, 1 NaH_2PO_4, 26.2 $NaHCO_3$, 11 glucose, and 0.2% of biocytin, saturated with 95% O_2 / 5% CO_2 at 30 ± 1°C. Details for whole-cell patch clamp recordings can be found in one of our previous publications (Ma et al., 2012). Cells were patched in voltage clamp mode and held at −70 mV. Only those recordings with a series resistance no higher than 20 MΩ and less than 20% variability were included in the subsequent data analyses. Cell membrane capacitance (Cm), input resistance (Rm) and time constant (**τ**) were calculated by applying a depolarizing step voltage command (5 mV) and using the membrane test function integrated in the pClamp11 software. sEPSCs were recorded for 90–120 sec in voltage clamp mode in the absence of $GABA_A$ receptor blockers as addition of these blockers would alter cortical pyramidal neuron excitability. Preservation of GABAergic synaptic inputs from local or distant projections is closer to the physiological condition. Further, addition of glutamate receptor antagonists, NBQX (10 μM) and AP-5 (50 μM), completely abolished spontaneous activity recorded at −70 mV (not shown). sEPSCs were analyzed off-line using the MiniAnalysis program (Synaptosoft Inc) with a threshold detection of 6 pA. This software was also used to calculate sEPSC frequency and amplitude. Resting membrane potential (RMP) was measured in current clamp mode with zero injection current. Resting membrane potential was adjusted to −70 mV via injection of positive current (50 – 100 pA) and then intrinsic excitability was examined using a series of depolarizing current pulses and constructing input-output (I-O) functions.

2.4. DiI staining

PrL-containing slices (200 μm) were prepared by the same procedure as slices for electrophysiological recordings. DiI staining was adapted from previous publications (Graziane et al., 2016; Mahmmoud et al., 2015). Brain slices were fixed with 1.5% paraformaldehyde (PFA) at room temperature for 30 min, and washed with phosphate-buffered saline (PBS) for 5 min, three times, and then mounted on a microglass. Slices were air-dried for 5 min and then DiI was brushed onto the slices with the aid of a Sutter Micromanipulator (MP-285) and its controller (MPC-200). The brain slices were then covered by a few drops of PBS and incubated at 37°C for 30 min. After a brief wash with PBS, the slices were incubated in 4% PFA for 30 min at room temperature. After washing

with PBS, 5 min for three times, a couple of drops of mounting medium (Molecular Probes™ ProLong™ Diamond Antifade Mountant) were added and slices were cover-slipped. The dendrites were imaged with a Nikon AR1 Confocal Microscope using a 63x oil-immersion objective and scanned at ~0.2 μm intervals along the z-axis. The collected z-stack images were processed using maximum intensity projection function. The images of pyramidal neurons with manually identifiable and quantifiable spines were used for the spine evaluation. We divided the spines into two large categories as explained in Fig. 3A. The spine qualification was manually performed with at least 4 randomly sampled secondary/tertiary dendrites (≥ 40 μm in length for each) per neuron and no less than 3 neurons per rat. Spine density (i.e., the number of spines per μm length of dendrite) for a specific neuron was calculated as the total number of identified spines divided by the total length of dendrites belonging to that neuron. The spine density for a specific rat was calculated by averaging the spine density of neurons analyzed in that rat.

Morphological exploration of basal, relative to apical, dendrites has been undertaken in laboratory animal models with chronic ethanol history, and with a general, although not exclusive, conclusion of significant effects of CIE on basal dendrites and spines arising from these dendrites, but not from apical branches (Cadete-Leite et al., 1990; Hamilton et al., 2010; Klenowski et al., 2016; Kroener et al., 2012). Therefore, together with the reliable identification of basal dendrites exclusively from PrL-L5 pyramidal neurons, the spine counting in this study was done in their basal, but not the apical dendrites.

2.5. Data Acquisition and Analysis

Data were collected either 2 days or 21 days after the last administration of water or ethanol. All results are shown as mean ± SEM. Each experiment was replicated in at least 4 rats (usually 2–4 cells per rat were recorded from 4–5 rats per group) for electrophysiological analysis. PrL pyramidal neurons, similar to those in other cerebral regions, have typical firing patterns (as shown in Figs. 1, 2, S1, S2), and morphologically have a triangle-shaped soma (Φ=15–25μm), with spiny basal and apical dendrites and a non-spiny axon. Those cells showing atypical electrophysiological properties (e.g., different firing patterns, outliers in terms of basic membrane properties, i.e., Cm, Rm, τ, and resting membrane potential), and / or atypical morphology based on biocytin staining (Ma et al., 2012) were excluded. Sample size is presented as “m/n” in Figs. 1–3, S1 and S2 and “n” in Fig.4, where “m” refers to the number of cells examined and “n” refers to the number of rats. Statistical significance was assessed using two-way ANOVA with repeated measures (Figs. 1D,F; S1D,F; 2D,F; S2D,F) or two-way ANOVA (Fig. 3B,C,E,F; 4C–J, Tables 1–5), followed by Bonferroni post-hoc tests.

3. Results

3.1. Membrane properties of PrL pyramidal neurons after CIW vs. CIE

Cell membrane capacitance (Cm), membrane input resistance (Rm), time constant (τ), and resting membrane potential (RMP) of the patched pyramidal neurons were measured as described in in the previous section. The data are summarized in Tables 1–4, and analyzed by two-way ANOVA. Data collected from the PrL-L5, but not from the PrL-L2, showed

statistically significant differences 21 days after CIW *vs.* CIE. Specifically, compared to the corresponding CIW controls, smaller Cm and higher Rm by Ado::CIE, were detected in the PrL-L5 on WD21. In contrast, larger Cm and lower Rm occurred by Adu::CIE. Smaller Cm and higher Rm would predict higher excitability. On the other hand, larger Cm and lower Rm would indicate reduced excitability. These predictions were supported by our excitability data described below.

3.2. Increased excitability in PrL-L5 pyramidal neurons 21 days, but not 2 days, after Ado::CIE

As shown in Fig. 1A, electrophysiological studies in PrL-containing coronal slices from rats treated by CIW/CIE during their adolescent stage were performed 2 days or 21 days after the last ethanol administration. Whole-cell patch clamp recordings of pyramidal neurons in PrL-L5 (Fig. 1B) in current clamp mode (example traces in Fig. 1C) 2 days after CIW *vs.* CIE treatment (decoded as WD2) showed no difference of spike number on WD2 (Fig. 1D). However, an injection current-dependent increase of spike number on WD21 was detected in Ado::CIE, relative to that in Ado::CIW (Fig. 1E, F). Thus, a delayed effect of Ado::CIE on PrL-L5 excitability is indicated by our data demonstrating that a prolonged withdrawal period is necessary for the progressive emergence of Ado::CIE effects.

3.3. No differences of excitability in PrL-L2 pyramidal neurons after Ado::CIW vs. Ado::CIE

As shown in Fig. S1A, the same slices used in data collection for PrL-L5 excitability after Ado::CIW or Ado::CIE were used in parallel to assess the PrL-L2 (Fig. S1B) excitability. Effects of Ado::CIE on PrL-L2 excitability were not detected on WD2 (Fig. S1C,D) or WD21 (Fig. S1E,F). Thus, we conclude that the effects of Ado::CIE on the PrL excitability has layer-specificity. Excitability of PrL-L5 seems more susceptible than PrL-L2 to Ado::CIE, although it takes time to fully develop these effects.

3.4. Decreased excitability in PrL-L5 pyramidal neurons 21days, but not 2 days, after Adu::CIE

After a comprehensive evaluation of Ado::CIE (CIE on P28–45) on PrL excitability, we wondered if the effects of CIE on PrL are developmental stage-specific. Thus, additional experiments were done on rats treated by Adu::CIW or Adu::CIE (CIW/CIE on P70–88). As shown in Fig. 2A, whole-cell patch clamp recordings (Fig. 2B) were obtained from pyramidal neurons in PrL-L5. Although no significant effects were detected on WD2 after Adu::CIE (Fig. 2C,D), an injection current-dependent decrease of spike number on WD21 was detected in Adu::CIE, relative to the data collected in Adu::CIW rats (Fig. 2E, F). Our data suggest that the developmental stage when the binge alcohol exposure occurs greatly influences the excitability of PrL-L5. Interestingly, the effects of both Ado::CIE and Adu::CIE seem to be gradually unmasked by the passage of the withdrawal period.

3.5. No differences of excitability in PrL-L2 pyramidal neurons after Adu::CIW vs. Adu::CIE

As shown in Fig. S2A, the same slices used to collect data on PrL-L5 excitability after Adu::CIW or Adu::CIE were used for assessing PrL-L2 (Fig. S2B) excitability. Similar to Ado::CIE, effects of Adu::CIE on PrL-L2 excitability were not detected on WD2 (Fig. S2C,D) or WD21 (Fig. S2E,F). Thus, we conclude that the effects of CIE on the PrL excitability has layer-specificity. Excitability of PrL-L2 seems resistant to both Ado::CIE and Adu::CIE.

3.6. Effects of CIE on sEPSCs of PrL-L5 pyramidal neurons

Due to their sensitivity and changes of intrinsic excitability to the CIE treatment, PrL-L5 pyramidal neurons were further evaluated by recording the frequency and amplitude of sEPSCs using whole-cell patch clamp. As exemplified in Fig. 3A, Ado::CIE, but not Adu::CIE, significantly decreased the amplitude of the sEPSCs recorded from PrL-L5 pyramidal neurons at the early withdrawal stage (i.e., WD2, Fig. 3C), relative to the corresponding CIW controls. However, no changes of sEPSC frequency were detected in rats 2 days after either Ado::CIE or Adu::CIE (Fig. 3B). Interestingly, both the frequency and the amplitude of sEPSCs were affected by CIE after a prolonged withdrawal period (Fig. 3D–F). Specifically, adolescent CIE decreased both the frequency and the amplitude of sEPSCs recorded from PrL-L5 pyramidal neurons. On the contrary, Adu::CIE increased their frequency and amplitude. Thus, similar to the changes of intrinsic excitability, the effects of CIE on synaptic transmission in PrL-L5 pyramidal neurons were opposite between the 2 age groups and suggested intervention of pre- and post-synaptic mechanisms.

3.7. Effects of CIE on spine morphology of PrL-L5 pyramidal neurons

The number of available spines, related to membrane area, is one of the critical factors that determine the efficiency to integrate input signals. Thus, a more detailed morphological analysis was performed on PrL-L5 pyramidal neurons. Dil staining, which can efficiently fill up and label the spines, even those with narrow necks, was used to assess the number of available spines after CIW or CIE treatment. As shown in Fig. 4A, total spines in the pyramidal neurons consist of non-thin spines (i.e., the sum of stubby spines and mushroom spines) and thin-spines (i.e., the sum of long thin spines and filopodium spines). The quantification of total spines as well as the two breakdown categories showed interesting and interactive effects of CIE and age on spine morphology of Prl-L5 pyramidal neurons. Specifically, although, relative to the age-matched CIW controls, no changes of total spine density (Fig. 4C), non-thin spine density (Fig. 4D), or thin spine density (Fig 4E) were observed on WD2 after either Ado::CIE or Adu::CIE, CIE treatment affected the thin spine ratio (Fig. 4F) in an age-independent manner. Particularly, a statistically significant increase of thin spine ratio was detected 2 days after Ado::CIE.

Then, we looked into the morphological data on WD21 after CIW/CIE treatment. Total spine density (Fig. 4G) and non-thin spine density (Fig. 4H) were decreased after Ado::CIE but increased after Adu::CIE. However, no further significant differences of thin spine density were observed between CIW *vs.* CIE treatments or between Ado *vs.* Adu age groups (Fig. 4I). The thin spine ratio was increased after Ado::CIE but decreased after Adu::CIE

(Fig. 4J), which may be attributed to the changes of non-thin spines. Thus, the prolonged effects of Ado::CIE and Adu::CIE were assumed to be a consequence of non-thin spine decreases and non-thin spine increases, respectively.

4. Discussion

Our data on changes in intrinsic excitability of pyramidal neurons in the PrL demonstrated a high sensitivity of L5, relative to L2, to the CIE, regardless of whether the CIE was given during adolescence or early-adulthood. These pyramidal neurons showed significant alterations in intrinsic excitability on WD21 but not on WD2, indicating that it takes time for the excitability changes to develop after CIE. Compared to the corresponding CIW controls, both Ado::CIE and Adu::CIE on WD21 resulted in a significant change in the intrinsic excitability. More importantly, the effects were differential; Ado::CIE increased but Adu::CIE decreased the intrinsic excitability of PrL-L5 on WD21. The opposite alterations of excitability in PrL-L5 could be related to the developmental-stage dependent responsiveness of pyramidal neurons to (1) binge-like ethanol exposure, (2) the intermittence between binge sessions, and (3) prolonged withdrawal from CIE. Since significant alterations were detected on WD21 but not WD2 after either Ado::CIE or Adu::CIE, the third factor could be the case. The different alterations of the PrL-L5 after adolescent *vs.* early adult CIE may explain the different symptoms observed in the clinic, although it cannot be excluded that different neuronal alterations may be involved in similar symptoms in subjects with Ado::CIE *vs.* Adu::CIE. Although alterations of L5 excitability have been reported (Salling et al., 2018; Trantham-Davidson et al., 2017), our paper is the first to compare, in parallel, the excitability of L2 to confirm the layer specific contributions after adolescent binge alcohol exposure. No changes in PrL-L2 after 2 days after Adu::CIE was also supported by Pleil *et al.* (Pleil et al., 2015). We would also like to emphasize that PrL-L2 has been reported as a cortical substrate of alcohol exposure. For example, decreases of total spine density but increase of non-thin spine density in mPFC L2 pyramidal neurons were detected ~2 weeks after binge-like ethanol exposure during postnatal days 4–9 (Hamilton et al., 2015; Hamilton et al., 2010; Whitcher and Klintsova, 2008).

The intrinsic excitability of projecting pyramidal neurons can be determined by the amplitude of the action potential afterhyperpolarization (AHP), including both the fast AHP (fAHP), assumed to be mediated by large conductance (BK) calcium-activated potassium channels and the medium AHP (mAHP), assumed to be mediated by small conductance (SK) calcium-activated potassium channels (Ishikawa et al., 2009; Matthews et al., 2009; Shah et al., 2006). Ado::CIE induced changes of AHP have been reported previously in the mPFC (Cannady et al., 2018; Salling et al., 2018). The amplitudes of the fAHP (data not shown) and mAHP (Table. 5) were analyzed in the current study but no difference was detected between CIW *vs.* CIE. RMPs were not changed by CIE in the current study, although membrane hyperpolarization of pyramidal neurons in mPFC was reported after voluntary Ado::CIE (Salling et al., 2018). Thus, our data indicate that alterations in intrinsic excitability in PrL-L5 pyramidal neurons do not appear attributable to some of their electrophysiological properties (e.g.., AHP and RMP), although we cannot rule out that other ionic conductances could contribute to changes in excitability which has been reported before (Cannady et al., 2018). It is worth noting that, in the PrL-L5, smaller Cm and higher

Rm 21 days after Ado::CIE could also underlie higher excitability, and higher Cm and lower Rm 21 days after Adu::CIE in the PrL-L5 might underlie lower excitability. The effects of CIE, at either adolescent or early adult stage, on intrinsic excitability is injection current-dependent. In other words, differences of spike number between CIW vs. CIE were only observed at highly depolarized potentials induced at higher current intensities. Thus, the adaptations observed in passive membrane properties (e.g., Cm, Rm) may not fully explain the injection current-dependent effects of CIE on intrinsic excitability.

Synaptic adaptations, as another primary factor determining neuronal excitability (Crabtree et al., 2017; Pratt and Aizenman, 2007), were evaluated by measuring the frequency and amplitude of sEPSCs, and the morphology of postsynaptic spines. Significant changes of sEPSCs and spine morphologies (e.g., density and percent of thin spines) were detected on both WD2 and WD21 in Prl-L5 pyramidal neurons, indicating that synaptic activity readouts are more sensitive to the effects of CIE at the early withdrawal stage. Significant decreases of sEPSC amplitude and increase of thin spine ratio were detected 2 days after Ado::CIE, compared to those in Ado::CIW group. The size of spine heads is speculated to have a positive correlation with the number of available excitatory post-synaptic receptors on that spine, such as NMDA or AMPA receptors (Newpher and Ehlers, 2008). Due to the voltage-dependent blockade of NMDA receptors at −70 mV at which our sEPSCs were recorded, we assume the AMPA receptors are decreased 2 days after Ado::CIE. Consistent with our prediction, glutamatergic transmission was enhanced ~ 1 week after CIE (Varodayan et al., 2018). Interestingly, the NMDA but not AMPA component of EPSCs increased in mPFC-L5 pyramidal neurons immediately or 1-week after CIE (Kroener et al., 2012).

21 days after CIE, robust but opposite synaptic adaptations were observed in rats with a history of CIE at adolescent *and* early-adult stages. Decrease of sEPSC frequency and amplitude, and decrease of total spine density were observed 21 days after Ado::CIE, whereas increase of sEPSC frequency and amplitude, and increase of total spine density were observed 21 days after Adu:: CIE. Total spine density, as a measurement of postsynaptic structure and indicating the availability of synaptic contacts, is assumed to be responsible for both the frequency and amplitude of sEPSCs. We found lower density of non-thin spines and higher thin spine ratio 21 days after Ado::CIE, indicating less excitatory postsynaptic receptors in PrL-L5 pyramidal neurons, which also could explain the smaller amplitude of sEPSCs. Interestingly, our data from PrL-L5 in Ado::CIE rats are consistent with those collected from IL but not the PrL in previous studies (Jury et al., 2017; Trantham-Davidson et al., 2017), in which mice or Long-Evans rats received ethanol vapor exposure. Higher total spine density and lower thin spine ratio, as observed 21 days after Adu::CIE, indicates more synaptic contacts and more excitatory postsynaptic receptors in PrL-L5 pyramidal neurons, explaining the higher frequency and larger amplitude of sEPSCs 21 days after Adu::CIE. The current synaptic data from early-adult animals are consistent with Klenowski et al., 2016 who reported increases of total spine densities and sEPSC frequency in L5 pyramidal neurons, supporting that long-term alcohol use enhances excitatory synaptic transmission in mPFC L5 pyramidal neurons (Klenowski et al., 2016).

Total spine density can be affected by both spine pruning and spine sprouting processes. Considering no changes in total spine density, we assume that the increased thin spine ratio

2 days after Ado::CIE is a consequence of remodeling of existing non-thin spines but not sprouting of nascent spines, followed by a pruning process, which explains the decreases of total spines 21 days after Ado::CIE. Since total spine density increased 21 days after Adu::CIE, we assume the prolonged effects of Adu::CIE is to increase nascent synaptic contacts, which is further supported by the increased frequency and amplitude of sEPSCs. Compared to thin spines, which are fragile and easy to be re-shaped, non-thin spines, which are highly stable and resistant to the environmental stimuli, are predicted to serve as the "memory spines" to reliably store the information of previous experience for a long term (Bourne and Harris, 2007). Changes in non-thin spine density were detected 21 days after both Ado::CIE and Adu::CIE, indicating persistent synaptic changes after CIE, regardless of the developmental stage at either adolescence or early-adulthood. One point that needs clarification is that as the postsynaptic components, spines are not exclusively innervated by excitatory inputs. Spines can be categorized into at least 3 types, including (1) immature spines which are thin and long, (2) mature excitatory spines innervated by excitatory inputs only, and (3) double input spines innervated by both inhibitory and excitatory inputs (Villa et al., 2016). Villa et al. found that, compared to the excitatory inputs, inhibitory inputs showed significantly lower density, and higher dynamics.

The functional output of a brain region relies on the integration of the synaptic transmission and intrinsic excitability. We found that weakened synaptic transmission, which led to a lower probability of depolarization to the threshold of action potential generation, but increased intrinsic excitability in the PrL-L5 21 days after Ado::CIE, which facilitates firing. On the other hand, 21 days after Adu::CIE, strengthened synaptic transmission but decreased intrinsic excitability were detected. Our data from both Ado::CIE and Adu::CIE evidenced the *synapse-membrane homeostatic crosstalk* (SMHC) (Ishikawa et al., 2009; Wang et al., 2018), which postulates that an increase or decrease in excitatory synaptic strength induces a homeostatic decrease or increase in the intrinsic membrane excitability, respectively. Cocaine exposure was reported to disrupt SMHC regulation (Wang et al., 2018). Recognition of SMHC mechanisms will guide effective manipulations on the brain pre-exposed to CIE in future studies.

5. Conclusions

Effects of developmental stage-dependent and PrL layer-specific effects of CIE were investigated here. The PrL-L5, but not PrL-L2, is the potential substrate mediating the prolonged effects of CIE. Although both developmental stages are sensitive to the CIE treatment, the adolescents and the early adults responded to CIE in an opposite way. The translational significance of this study is that different treatments may need to be developed after Ado::CIE *vs.* Adu::CIE although both lead to prolonged consequences in brain function.

Supplementary Material

Refer to Web version on PubMed Central for supplementary material.

FUNDING

This work was supported by NIH grants (R01AA025784, P50AA017823, T32AA025606) and Brain & Behavior Research Foundation grant #24989.

REFERENCES

Bourne J, Harris KM, 2007 Do thin spines learn to be mushroom spines that remember? Curr Opin Neurobiol 17(3), 381–386. [PubMed: 17498943]

Cadete-Leite A, Alves MC, Paula-Barbosa MM, Uylings HB, Tavares MA, 1990 Quantitative analysis of basal dendrites of prefrontal pyramidal cells after chronic alcohol consumption and withdrawal in the adult rat. Alcohol Alcohol 25(5), 467–475. [PubMed: 2088349]

Cannady R, Rinker JA, Nimitvilai S, Woodward JJ, Mulholland PJ, 2018 Chronic Alcohol, Intrinsic Excitability, and Potassium Channels: Neuroadaptations and Drinking Behavior. Handb Exp Pharmacol 248, 311–343. [PubMed: 29374839]

Cooper JA, 2008 A mechanism for inside-out lamination in the neocortex. Trends Neurosci 31(3), 113–119. [PubMed: 18255163]

Crabtree GW, Sun Z, Kvajo M, Broek JA, Fenelon K, McKellar H, Xiao L, Xu B, Bahn S, O'Donnell JM, Gogos JA, 2017 Alteration of Neuronal Excitability and Short-Term Synaptic Plasticity in the Prefrontal Cortex of a Mouse Model of Mental Illness. J Neurosci 37(15), 4158–4180. [PubMed: 28283561]

D'Souza RD, Burkhalter A, 2017 A Laminar Organization for Selective Cortico-Cortical Communication. Front Neuroanat 11, 71. [PubMed: 28878631]

Graziane NM, Sun S, Wright WJ, Jang D, Liu Z, Huang YH, Nestler EJ, Wang YT, Schluter OM, Dong Y, 2016 Opposing mechanisms mediate morphine- and cocaine-induced generation of silent synapses. Nat Neurosci 19(7), 915–925. [PubMed: 27239940]

Hamilton GF, Criss KJ, Klintsova AY, 2015 Voluntary exercise partially reverses neonatal alcohol-induced deficits in mPFC layer II/III dendritic morphology of male adolescent rats. Synapse 69(8), 405–415. [PubMed: 25967699]

Hamilton GF, Whitcher LT, Klintsova AY, 2010 Postnatal binge-like alcohol exposure decreases dendritic complexity while increasing the density of mature spines in mPFC Layer II/III pyramidal neurons. Synapse 64(2), 127–135. [PubMed: 19771589]

Harris KD, Shepherd GM, 2015 The neocortical circuit: themes and variations. Nat Neurosci 18(2), 170–181. [PubMed: 25622573]

Ishikawa M, Mu P, Moyer JT, Wolf JA, Quock RM, Davies NM, Hu XT, Schluter OM, Dong Y, 2009 Homeostatic synapse-driven membrane plasticity in nucleus accumbens neurons. J Neurosci 29(18), 5820–5831. [PubMed: 19420249]

Jury NJ, Pollack GA, Ward MJ, Bezek JL, Ng AJ, Pinard CR, Bergstrom HC, Holmes A, 2017 Chronic Ethanol During Adolescence Impacts Corticolimbic Dendritic Spines and Behavior. Alcohol Clin Exp Res 41(7), 1298–1308. [PubMed: 28614590]

Klenowski PM, Fogarty MJ, Shariff M, Belmer A, Bellingham MC, Bartlett SE, 2016 Increased Synaptic Excitation and Abnormal Dendritic Structure of Prefrontal Cortex Layer V Pyramidal Neurons following Prolonged Binge-Like Consumption of Ethanol. eNeuro 3(6).

Kroener S, Mulholland PJ, New NN, Gass JT, Becker HC, Chandler LJ, 2012 Chronic alcohol exposure alters behavioral and synaptic plasticity of the rodent prefrontal cortex. PLoS One 7(5), e37541. [PubMed: 22666364]

Kyzar EJ, Zhang H, Pandey SC, 2019 Adolescent Alcohol Exposure Epigenetically Suppresses Amygdala Arc Enhancer RNA Expression to Confer Adult Anxiety Susceptibility. Biol Psychiatry 85(11), 904–914. [PubMed: 30827484]

Lefort S, Tomm C, Floyd Sarria JC, Petersen CC, 2009 The excitatory neuronal network of the C2 barrel column in mouse primary somatosensory cortex. Neuron 61(2), 301–316. [PubMed: 19186171]

Ma YY, Cepeda C, Chatta P, Franklin L, Evans CJ, Levine MS, 2012 Regional and cell-type-specific effects of DAMGO on striatal D1 and D2 dopamine receptor-expressing medium-sized spiny neurons. ASN neuro 4(2).

Ma YY, Lee BR, Wang X, Guo C, Liu L, Cui R, Lan Y, Balcita-Pedicino JJ, Wolf ME, Sesack SR, Shaham Y, Schluter OM, Huang YH, Dong Y, 2014 Bidirectional modulation of incubation of cocaine craving by silent synapse-based remodeling of prefrontal cortex to accumbens projections. Neuron 83(6), 1453–1467. [PubMed: 25199705]

Mahmmoud RR, Sase S, Aher YD, Sase A, Groger M, Mokhtar M, Hoger H, Lubec G, 2015 Spatial and Working Memory Is Linked to Spine Density and Mushroom Spines. PLoS One 10(10), e0139739. [PubMed: 26469788]

Matthews EA, Linardakis JM, Disterhoft JF, 2009 The fast and slow afterhyperpolarizations are differentially modulated in hippocampal neurons by aging and learning. J Neurosci 29(15), 4750–4755. [PubMed: 19369544]

National Institute on Alcohol Abuse and Alcoholism, N., 2017 Underage Drinking.

Newpher TM, Ehlers MD, 2008 Glutamate receptor dynamics in dendritic microdomains. Neuron 58(4), 472–497. [PubMed: 18498731]

Paxinos G, Watson C, 2007 The rat brain in stereotaxic coordinates (6th edition).

Petanjek Z, Judas M, Simic G, Rasin MR, Uylings HB, Rakic P, Kostovic I, 2011 Extraordinary neoteny of synaptic spines in the human prefrontal cortex. Proc Natl Acad Sci U S A 108(32), 13281–13286. [PubMed: 21788513]

Pleil KE, Lowery-Gionta EG, Crowley NA, Li C, Marcinkiewcz CA, Rose JH, McCall NM, Maldonado-Devincci AM, Morrow AL, Jones SR, Kash TL, 2015 Effects of chronic ethanol exposure on neuronal function in the prefrontal cortex and extended amygdala. Neuropharmacology 99, 735–749. [PubMed: 26188147]

Pratt KG, Aizenman CD, 2007 Homeostatic regulation of intrinsic excitability and synaptic transmission in a developing visual circuit. J Neurosci 27(31), 8268–8277. [PubMed: 17670973]

Rolls ET, 2016 Cerebral Cortex: Principles of Operation

Sakharkar AJ, Kyzar EJ, Gavin DP, Zhang H, Chen Y, Krishnan HR, Grayson DR, Pandey SC, 2019 Altered amygdala DNA methylation mechanisms after adolescent alcohol exposure contributes to adult anxiety and alcohol drinking. Neuropharmacology, 107679. [PubMed: 31229451]

Salling MC, Skelly MJ, Avegno E, Regan S, Zeric T, Nichols E, Harrison NL, 2018 Alcohol Consumption during Adolescence in a Mouse Model of Binge Drinking Alters the Intrinsic Excitability and Function of the Prefrontal Cortex through a Reduction in the Hyperpolarization-Activated Cation Current. J Neurosci 38(27), 6207–6222. [PubMed: 29915134]

Shah MM, Javadzadeh-Tabatabaie M, Benton DC, Ganellin CR, Haylett DG, 2006 Enhancement of hippocampal pyramidal cell excitability by the novel selective slow-afterhyperpolarization channel blocker 3-(triphenylmethylaminomethyl)pyridine (UCL2077). Mol Pharmacol 70(5), 1494–1502. [PubMed: 16877678]

Shan L, Galaj E, Ma YY, 2019 Nucleus accumbens shell small conductance potassium channels underlie adolescent ethanol exposure-induced anxiety. Neuropsychopharmacology.

Sloan F, Grossman D, Platt A, 2011 Heavy episodic drinking in early adulthood and outcomes in midlife. J Stud Alcohol Drugs 72(3), 459–470. [PubMed: 21513683]

Spear LP, Swartzwelder HS, 2014 Adolescent alcohol exposure and persistence of adolescent-typical phenotypes into adulthood: a mini-review. Neuroscience and biobehavioral reviews 45, 1–8. [PubMed: 24813805]

Spiga S, Talani G, Mulas G, Licheri V, Fois GR, Muggironi G, Masala N, Cannizzaro C, Biggio G, Sanna E, Diana M, 2014 Hampered long-term depression and thin spine loss in the nucleus accumbens of ethanol-dependent rats. Proc Natl Acad Sci U S A 111(35), E3745–3754. [PubMed: 25122682]

Substance Abuse and Mental Health Services Administration, S., 2015 Key Substance Use and Mental Health Indicators in the United States: Results from the 2015. National Survey on Drug Use and Health.

Trantham-Davidson H, Centanni SW, Garr SC, New NN, Mulholland PJ, Gass JT, Glover EJ, Floresco SB, Crews FT, Krishnan HR, Pandey SC, Chandler LJ, 2017 Binge-Like Alcohol Exposure During

Adolescence Disrupts Dopaminergic Neurotransmission in the Adult Prelimbic Cortex. Neuropsychopharmacology 42(5), 1024–1036. [PubMed: 27620551]

Varodayan FP, Sidhu H, Kreifeldt M, Roberto M, Contet C, 2018 Morphological and functional evidence of increased excitatory signaling in the prelimbic cortex during ethanol withdrawal. Neuropharmacology 133, 470–480. [PubMed: 29471053]

Villa KL, Berry KP, Subramanian J, Cha JW, Chan Oh W, Kwon HB, Kubota Y, So PT, Nedivi E, 2016 Inhibitory Synapses Are Repeatedly Assembled and Removed at Persistent Sites In Vivo. Neuron 90(3), 662–664.

Viner RM, Taylor B, 2007 Adult outcomes of binge drinking in adolescence: findings from a UK national birth cohort. J Epidemiol Community Health 61(10), 902–907. [PubMed: 17873228]

Wang J, Ishikawa M, Yang Y, Otaka M, Kim JY, Gardner GR, Stefanik MT, Milovanovic M, Huang YH, Hell JW, Wolf ME, Schluter OM, Dong Y, 2018 Cascades of Homeostatic Dysregulation Promote Incubation of Cocaine Craving. J Neurosci 38(18), 4316–4328. [PubMed: 29626166]

Whitcher LT, Klintsova AY, 2008 Postnatal binge-like alcohol exposure reduces spine density without affecting dendritic morphology in rat mPFC. Synapse 62(8), 566–573. [PubMed: 18512209]

Witt ED, 2010 Research on alcohol and adolescent brain development: opportunities and future directions. Alcohol 44(1), 119–124. [PubMed: 20113880]

Highlights:

- Layer 5 (L5) but not layer 2 (L2) pyramidal neurons in the prelimbic cortex (PrL) showed developmental stage-dependent effects of chronic intermittent ethanol (CIE).
- No changes in PrL-L5 neurons were detected 2 days after either adolescent or early-adult CIE.
- Intrinsic excitability of PrL-L5 pyramidal neurons was increased by adolescent CIE, but decreased by early-adult CIE after a protracted withdrawal period.
- Synaptic transmission and the density of total spines and non-thin spines in PrL-L5 pyramidal neurons were decreased 21 days after adolescent CIE, but increased 21 days after early-adult CIE.

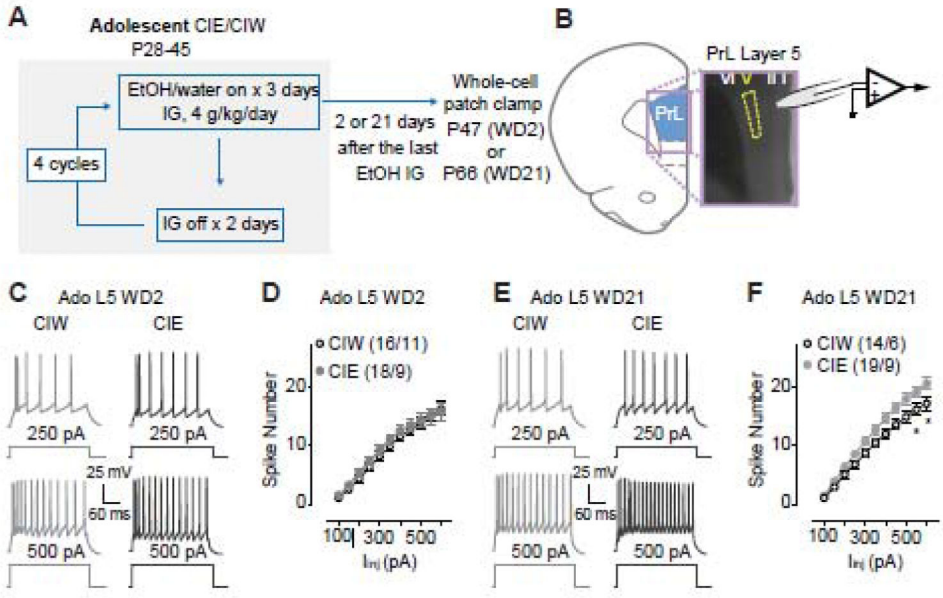

Figure 1. Increased excitability of layer 5 pyramidal neurons in the PrL 21 days, but not 2 days, after Ado::CIE procedure

A, Detailed experimental time line.

B, Location of whole-cell patch clamp recordings in PrL-L5.

C, Example traces of action potentials elicited by 250 and 500 pA current injections to a PrL-L5 pyramidal neuron 2 days after Ado::CIW and Ado::CIE.

D, Summarized data showing no changes of spike number recorded from PrL-L5 pyramidal neurons 2 days after the Ado::CIW *vs.* Ado::CIE (I_{inj} × CIW/CIE interaction $F_{10,320}$=0.4, p=0.92, CIW/CIE $F_{1,32}$=0.4, p=0.55, cell-based; I_{inj} × CIW/CIE interaction $F_{10,180}$=0.3 p=0.98, CIW/CIE $F_{1,18}$=0.4, p=0.53, animal-based).

E, Example traces of action potentials elicited by 250 and 500 pA current injections to a PrL-L5 pyramidal neuron 21 days after Ado::CIW and Ado::CIE.

F, Summarized data showing an increased excitability of PrL-L5 pyramidal neurons 21 days after Ado::CIE (I_{inj} × CIW/CIE interaction $F_{10,310}$=2.6, p<0.01, CIW/CIE $F_{1,31}$=4.9, p=0.03, cell-based; I_{inj} × CIW/CIE interaction $F_{10,130}$=3.1, p<0.01, CIW/CIE $F_{1,13}$=5.1, p=0.04, animal-based).

Data were analyzed by two-way ANOVA with repeated measures (**D**, **F**), followed by Bonferroni post-hoc tests. n/m, the number of cells/animals for data collection. *, p<0.05, CIW *vs.* CIE at the specific injection current.

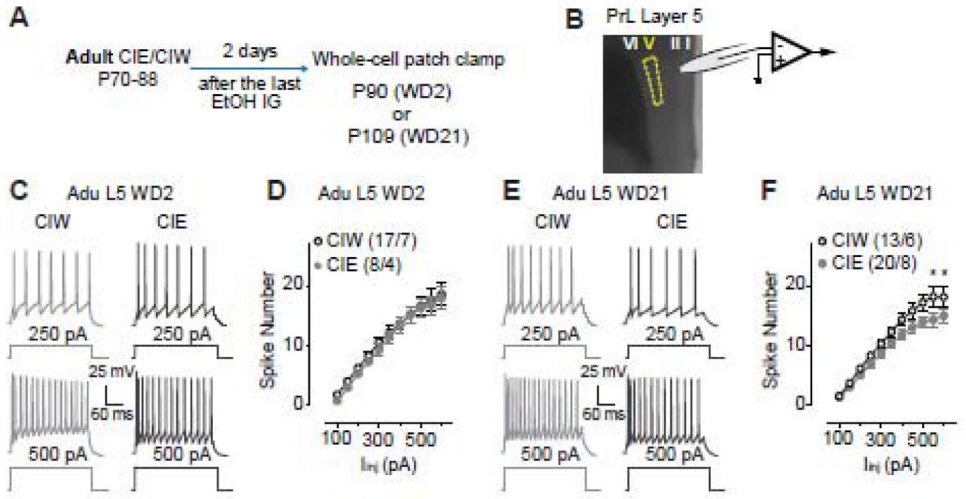

Figure 2. Decreased excitability of layer 5 pyramidal neurons in the PrL 21 days, but not 2 days, after Adu::CIE

A, Experimental time line, see more details in Fig. 1A.

B, Location of whole-cell patch clamp recordings in PrL-L5.

C, Example traces of action potentials elicited by 250 and 500 pA current injections to a PrL-L5 pyramidal neuron 2 days after Adu::CIW and Adu::CIE.

D, Summarized data showing no changes of spike number recorded from PrL-L5 pyramidal neurons 2 days after the Adu::CIW vs. Adu::CIE (I_{inj} × CIW/CIE interaction $F_{10,200}$=0.1, p=0.99, CIW/CIE $F_{1,20}$=0.3, p=0.59, cell -based; I_{inj} × CIW/CIE interaction $F_{10,90}$=0.5, p=0.90, CIW/CIE $F_{1,9}$=0.2, p=0.66, animal -based).

E, Example traces of action potentials elicited by 250 and 500 pA current injections to a PrL-L5 pyramidal neuron 21 days after Adu::CIW and Adu::CIE.

F, Summarized data showing a decreased excitability of PrL-L5 pyramidal neurons 21 days after Adu::CIE (I_{inj} × CIW/CIE interaction $F_{10,310}$=2.2, p=0.02, CIW/CIE $F_{1,31}$=3.4, p=0.07, cell -based; I_{inj} × CIW/CIE interaction $F_{10,120}$=2.0, p=0.03, CIW/CIE $F_{1,12}$=3.1, p=0.10, animal -based).

Data were analyzed by two-way ANOVA with repeated measures (**D**, **F**), followed by Bonferroni post-hoc tests. n/m, the number of cells/animals for data collection. *, p<0.05, CIW *vs.* CIE at the specific current injection.

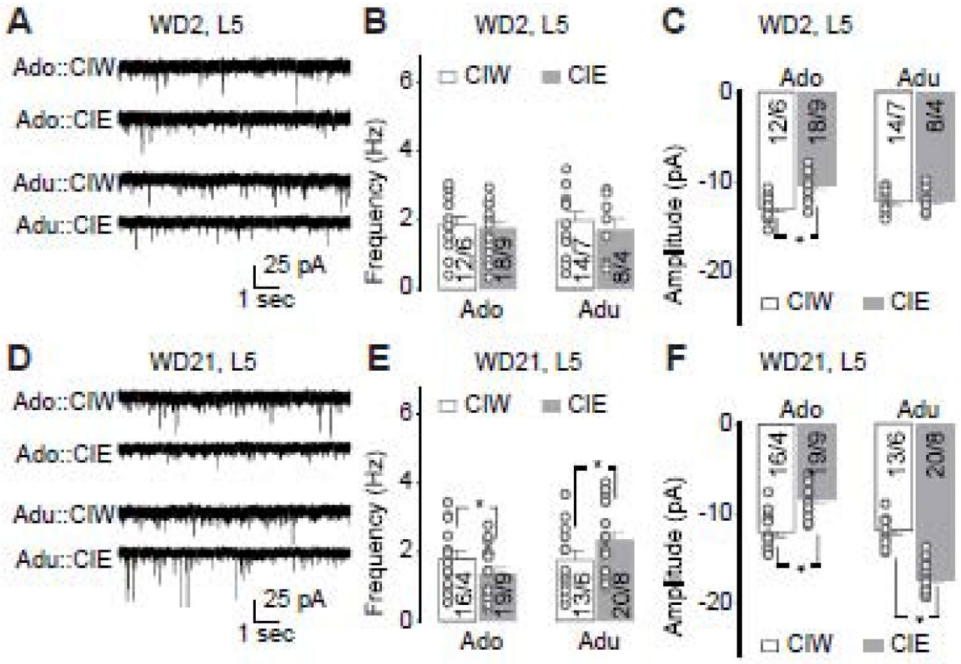

Figure 3. Effects of CIE on sEPSCs recorded from PrL-L5 pyramidal neurons

A, Representative traces of sEPSCs 2 days after adolescent CIW/CIE treatment and early-adult CIW/CIE treatment.

B, Summarized data showing no effects of adolescent or early-adult CIE on the frequency of sEPSCs (CIW/CIE × Ado/Adu interaction $F_{1,48}$=0.1, p=0.72, CIW/CIE $F_{1,48}$=0.6, p=0.46, Ado/Adu $F_{1,48}$<0.1, p=0.87, cell-based; CIW/CIE × Ado/Adu interaction $F_{1,22}$=0.3, p=0.61, CIW/CIE $F_{1,22}$=0.1, p=0.71, Ado/Adu $F_{1,22}$=0.1, p=0.72, animal-based).

C, Summarized data showing significant decrease of sEPSC amplitude 2 days after adolescent, but not early-adult, CIE (CIW/CIE × Ado/Adu interaction $F_{1,48}$=8.3, p<0.01, CIW/CIE $F_{1,48}$=11.5, p<0.01, Ado/Adu $F_{1,48}$=1.0, p=0.32, cell-based; CIW/CIE × Ado/Adu interaction $F_{1,22}$=8.4, p=0.01, CIW/CIE $F_{1,22}$=11.7, p<0.01, Ado/Adu $F_{1,22}$=1.2, p=0.29, animal-based).

D, Representative traces of sEPSCs 21 days after adolescent CIW/CIE treatment and early-adult CIW/CIE treatment.

E, Summarized data showing that sEPSC frequency significantly decreased and increased 2 days after adolescent and early-adult CIE, respectively (CIW/CIE × Ado/Adu interaction $F_{1,62}$=4.4, p=0.04, CIW/CIE $F_{1,62}$=0.1, p=0.79, Ado/Adu $F_{1,62}$=3.9, p=0.05, cell-based; CIW/CIE × Ado/Adu interaction $F_{1,25}$=7.8, p=0.01, CIW/CIE $F_{1,25}$<0.1, p=0.85, Ado/Adu $F_{1,25}$=6.5, p=0.02, animal-based).

F, Summarized data showing that sEPSC amplitude significantly decreased and increased 2 days after adolescent and early-adult CIE, respectively (CIW/CIE × Ado/Adu interaction $F_{1,62}$=108.3, p<0.01, CIW/CIE $F_{1,62}$=4.4, p=0.04, Ado/Adu $F_{1,62}$=99.8, p<0.01, cell-based; CIW/CIE × Ado/Adu interaction $F_{1,25}$=116.5, p<0.01, CIW/CIE $F_{1,25}$=4.7, p=0.04, Ado/Adu $F_{1,25}$=102.8, p<0.01, animal-based).

Data were analyzed by two-way ANOVA (**B**,**C**,**E**,**F**), followed by Bonferroni post-hoc tests. n/m, the number of cells/animals.

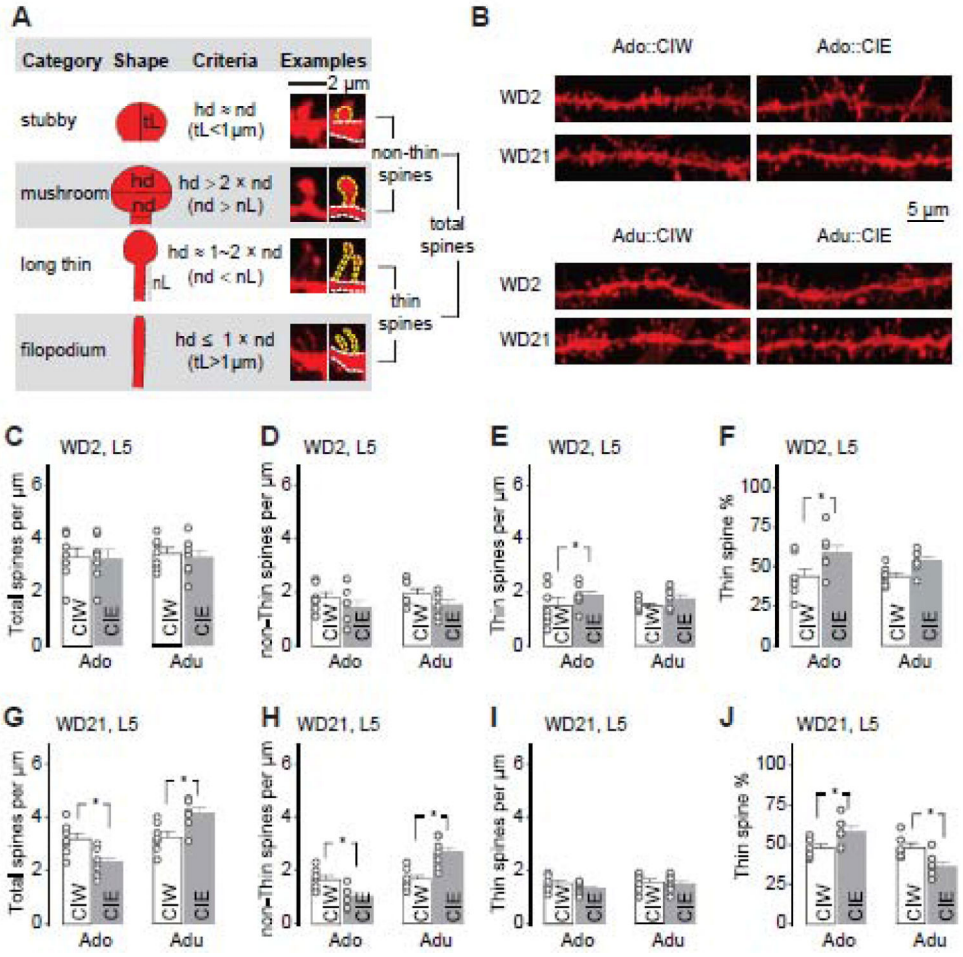

Figure 4. Effects of CIE on spine morphology of PrL-L5 pyramidal neurons

A, Adapted criteria for 4 types of spines from Spiga et al, 2014 (Spiga et al., 2014) and example spines for each type.

B, Example DiI-stained spines in PrL-L5 pyramidal neurons 2 and 21 days after CIW or CIE treatment during the adolescent and early-adult stages, respectively.

C–F, Summarized data showing the spine density of total spines (**C**), non-thin spines (**D**) and thin spines (**E**), as well as the thin spine % among total spines (**F**) 2 days after CIW or CIE treatment. Neither CIE treatment nor the age factor significantly affected total spine density (**C**, CIW/CIE × Ado/Adu interaction $F_{1,24}$<0.1, p=0.84, CIW/CIE $F_{1,24}$=0.1, p=0.74, Ado/Adu $F_{1,24}$=0.1, p=0.78), non-thin spine density (**D**, CIW/CIE × Ado/Adu interaction $F_{1,24}$<0.1, p=0.85, CIW/CIE $F_{1,24}$=5.5, p=0.03, Ado/Adu $F_{1,24}$=1.0, p=0.32), or thin spine density (**E**, CIW/CIE × Ado/Adu interaction $F_{1,24}$=0.2 p=0.48, CIW/CIE $F_{1,24}$=3.1, p=0.09, Ado/Adu $F_{1,24}$=0.32, p=0.58). CIE treatment, but not the age factor, significantly affect the thin spine ratio (**F**, CIW/CIE × Ado/Adu interaction $F_{1,24}$=0.4, p=0.54, CIW/CIE $F_{1,24}$=9.8, p<0.01, Ado/Adu $F_{1,24}$=0.4, p=0.54)

G–J, Summarized data showing the spine density of total spines (**G**), non-thin spines (**H**) and thin spines (**I**), as well as the thin spine % among total spines (**J**) 21 days after CIW or CIE treatment. Total spine density was decreased after Ado::CIE but increased after

Adu::CIE (**G**, CIW/CIE × Ado/Adu interaction $F_{1,24}$=18.4, p<0.01, CIW/CIE $F_{1,24}$<0.1, p=0.95, Ado/Adu $F_{1,24}$=21.4, p<0.01). Similarly, Ado::CIE and Adu::CIE significantly decreased and increase the non-Thin spine density, respectively (**H**, CIW/CIE × Ado/Adu interaction $F_{1,24}$=24.8, p<0.01, CIW/CIE $F_{1,24}$=0.9, p=0.36, Ado/Adu $F_{1,24}$=26.1, p<0.01). No significant differences of thin spine density were observed between CIW *vs.* CIE treatments or between Ado *vs.* Adu age groups (**I**, CIW/CIE × Ado/Adu interaction $F_{1,24}$=0.5 p=0.48, CIW/CIE $F_{1,24}$=1.7, p=0.20, Ado/Adu $F_{1,24}$=1.4, p=0.25). Thin spine ratio was increased after Ado::CIE but decreased after Adu::CIE (**J**, CIW/CIE × Ado/Adu interaction $F_{1,24}$=15.8, p<0.01, CIW/CIE $F_{1,24}$=0.1, p=0.72, Ado/Adu $F_{1,24}$=15.4, p<0.01). Data were analyzed by two-way ANOVA (**C–J**), followed by Bonferroni post-hoc tests. Data collections were made on 7 rats in each group.

Table 1.

Effects of CIE on Membrane Capacitance (Cm) of PrL pyramidal neurons

Cm (pF)		Ado::L5			Ado::L2	
		CIW	CIE		CIW	CIE
	WD2	135±12	132±11		187±9	204±11
	WD21	137±9	122±6*		209±7	203±9
		Adu::L5			Adu::L2	
		CIW	CIE		CIW	CIE
	WD2	122±12	139±14		200±10	207±11
	WD21	119±6	156±13*		200±6	200±12

Membrane properties and amplitude of mAHP of pyramidal neurons after CIW *vs*. CIE treatment Data were analyzed by two-way ANOVA, followed by Bonferroni post-hoc tests. Statistical significances were detected in those shaded in gray panel.

*, $p<0.05$ by comparing CIW *vs*. CIE.

Table 2.

Effects of CIE on Membrane Resistance (Rm) of PrL pyramidal neurons

Rm (MΩ)		Ado::L5			Ado::L2	
		CIW	CIE		CIW	CIE
	WD2	228±27	205±27		145±9	139±7
	WD21	182±25	239±18 *		125±7	135±12
		Adu::L5			Adu::L2	
		CIW	CIE		CIW	CIE
	WD2					
		220±17	212±27		118±9	131±12
	WD21	226±20	191±23		124±5	122±8

Membrane properties and amplitude of mAHP of pyramidal neurons after CIW *vs*. CIE treatment Data were analyzed by two-way ANOVA, followed by Bonferroni post-hoc tests. Statistical significances were detected in those shaded in gray panel.

*, $p<0.05$ by comparing CIW *vs*. CIE.

Table 3.

Effects of CIE on Tau values of PrL pyramidal neurons

Tau (ms)		Ado::L5			Ado::L2	
		CIW	CIE		CIW	CIE
	WD21	1.7±0.1	1.7±0.1		2.4±0.1	2.5±0.1
		1.6±0.1	1.5±0.1		2.7±0.1	2.5±0.1
		Adu::L5			Adu::L2	
		CIW	CIE		CIW	CIE
	WD2	1.6±0.2	1.8±0.1		2.6±0.2	2.7±0.1
	WD21	1.4±0	1.8±0.1		2.5±0.1	2.5±0.1

Membrane properties and amplitude of mAHP of pyramidal neurons after CIW *vs*. CIE treatment Data were analyzed by two-way ANOVA, followed by Bonferroni post-hoc tests. Statistical significances were detected in those shaded in gray panel.

*, $p<0.05$ by comparing CIW *vs*. CIE.

Table 4.

Effects of CIE on Resting Membrane Potential (RMP) of PrL pyramidal neurons

RMP (mV)		Ado::L5			Ado::L2	
		CIW	CIE		CIW	CIE
	WD2	−71.2±0.9	−72.5±0.7		−71.3±0.6	−71.1±0.7
	WD21	−71.2±0.7	−71.7±0.7		−72.4±0.8	−71.6±0.7
		Adu::L5			Adu::L2	
		CIW	CIE		CIW	CIE
	WD2	−72.6±0.7	−71.3±0.6		−72.6±0.8	−72.8±1
	WD21	−71.4±0.7	−72.6±0.6		−70.6±0.8	−71.9±0.7

Membrane properties and amplitude of mAHP of pyramidal neurons after CIW *vs*. CIE treatment Data were analyzed by two-way ANOVA, followed by Bonferroni post-hoc tests. Statistical significances were detected in those shaded in gray panel.

*, p<0.05 by comparing CIW *vs*. CIE.

Table 5.

Effects of CIE on mAHP amplitude of PrL pyramidal neurons

mAHP (mV)		Ado::L5			Ado::L2	
		CIW	CIE		CIW	CIE
	WD2	−12.8±0.6	−11.7±0.8		−10.8±0.5	−11.0±0.6
	WD21	−11.7±0.7	−11.8±0.7		−10.2±0.7	−10.5±0.8
		Adu::L5			Adu::L2	
		CIW	CIE		CIW	CIE
	WD2	−12.3±0.6	−12.0±0.7		−11.2±0.6	−10.7±0.6
	WD21	−11.8±0.7	−12.2±0.5		−10.6±0.8	−11.3±0.5

Membrane properties and amplitude of mAHP of pyramidal neurons after CIW *vs*. CIE treatment Data were analyzed by two-way ANOVA, followed by Bonferroni post-hoc tests. Statistical significances were detected in those shaded in gray panel.

*, $p<0.05$ by comparing CIW *vs*. CIE.